

CARBON ISOTOPE RATIOS IN FIELD POPULATION II GIANT STARS

CHRISTOPHER SNEDEN¹

Department of Astronomy and McDonald Observatory, University of Texas at Austin

CATHERINE A. PILACHOWSKI

Kitt Peak National Observatory, National Optical Astronomy Observatories

AND

DON A. VANDENBERG

Physics Department, University of Victoria

Received 1985 December 16; accepted 1986 May 2

ABSTRACT

Carbon isotope ratios have been derived from high-resolution spectra of the CH G-band in 15 very metal-poor Population II giant stars and two similar dwarf stars. Many of the giants possess very low $^{12}\text{C}/^{13}\text{C}$ ratios, some approaching the CN cycle equilibrium value. The metal-poor dwarfs do not have detectable ^{13}CH features; thus the low carbon isotope ratios in the giants probably are due to their internal evolutions. These results strongly support the idea that at least part of the anomalously low C/N values in Population II giants arises from very efficient mixing of their envelopes into the CN cycle burning layers. Detailed calculations of the expected CNO surface abundances in Population II giants in different evolutionary states have been performed. These computations demonstrate that the observed carbon isotope ratios cannot be produced during the first dredge-up mixing phases in low-mass, low metal abundance stars. Numerical experiments show that theoretical and observational results can be brought into agreement with artificially induced extra mixing. An agent to provoke this additional mixing has not been identified with certainty yet, although internal stellar rotation is a promising candidate.

Subject headings: stars: abundances — stars: evolution — stars: interiors — stars: late-type — stars: Population II

I. INTRODUCTION

Abundances and isotopic ratios of the light elements carbon, nitrogen, and oxygen in the atmospheres of giants of all stellar populations contain vital clues to the evolutionary histories of these stars. The spectra of nearby Population I disk stars have been analyzed extensively at both high and low resolution. All major studies have reached nearly the same conclusions: most stars, during the first ascent of the giant branch, will develop deep convective envelopes and will mix their core CN-cycle hydrogen burning products with their envelope layers. Therefore their original carbon contents will drop by factors of ~ 2 , their nitrogen abundances will rise by corresponding amounts, the carbon isotope ratios will decrease from ~ 90 to 20–30, and their oxygen contents will remain constant (e.g., see Lambert and Ries 1981; Kjergaard *et al.* 1982; Iben and Renzini 1984). Theory and observations are in agreement that for typical Population I giants, $\log(C/N) \approx 0.2$.

Until recently, Population II halo giants had been studied less extensively, because of their relative faintness. Over the last decade, however, some CNO abundance results have become available. Sneden (1973, 1974), Barbuy (1983), and Kraft *et al.* (1982; hereinafter K82) employed spectroscopic data of various resolutions and signal-to-noise values to demonstrate the existence of nitrogen overabundances and carbon underabundances in very metal-poor field giants. However, the C/N

ratios derived for Population II giants are smaller than those of similar Population I stars, exhibit more star-to-star scatter, and may be functions of the overall metallicities. Also, Population II giants and dwarfs possess large O/Fe ratios compared with the Population I stars.

In Table 1 we summarize the results of some of the major surveys of CNO in Population I and Population II stars. Clearly, differences exist in these abundances among the different stellar classes. However, some caution must be used in the interpretation of the abundances listed in Table 1. Various investigators derived stellar atmosphere parameters under quite different assumptions, and have employed different molecular parameters for the analysis of different molecular bands; thus some unknown offsets in the entries for Table 1 undoubtedly exist. For example, Langer, Kraft, and Friel (1985) and Langer (1985) have used their syntheses of CN bands in some M5 giants to suggest that the earlier sets of C and N abundances derived by their group (e.g., K82) should be revised by an addition of 0.2 dex to all $[C/Fe]$ values and a subtraction of 0.2 dex from all $[N/Fe]$ values. If these proposed shifts are correct, then obviously the K82 values for $\log(C/N)$ given in Table 1 should be increased by 0.4 dex. Therefore, the comparison with more metal-rich populations could change substantially. At first glance, the corrected C/N ratios of the moderately metal-poor giants (Cottrell and Sneden 1985). The substantial differences with the disk stars might exist then only in the most extremely metal-poor giants. The suggested shifts for the C and N abundances determined by Kraft and collaborators are not certain, and other, perhaps stronger, arguments, could be made for scale uncertainties in the results of any of the other studies shown in Table 1. The reader should bear these

¹ Visiting Astronomer, Kitt Peak National Observatory, National Optical Astronomy Observatories, operated by the Association of Universities for Research in Astronomy, under contract with the National Science Foundation.

TABLE 1
CNO ABUNDANCES IN POPULATION I AND POPULATION II GIANT STARS

[Fe/H]	[C/Fe]	[N/Fe]	log(C/N)	[O/Fe]	Reference
-0.10 ± 0.20	-0.35 ± 0.15	$+0.20 \pm 0.15$	$+0.15 \pm 0.25$	-0.15 ± 0.15	1
-0.10 ± 0.25	-0.20 ± 0.15	$+0.10 \pm 0.15$	$+0.38 \pm 0.20$	-0.05 ± 0.15	2
-0.50 ± 0.15	-0.10 ± 0.11	$+0.05 \pm 0.20$	$+0.55 \pm 0.25$	$+0.10 \pm 0.15$	3
-1.80 ± 0.15	-0.50 ± 0.30	-0.05 ± 0.25	$+0.25 \pm 0.35$...	4
-2.40 ± 0.20	-0.65 ± 0.35	$+0.15 \pm 0.30$	-0.20 ± 0.50	...	5
-2.40 ± 0.25	-0.30 ± 0.45	$+0.75 \pm 0.30$	-0.35 ± 0.55	$+0.70 \pm 0.10$	6
...	$+0.50 \pm 0.25$	7

REFERENCES.—(1) Lambert and Ries 1981, with entries adjusted to reflect a decrease in the effective temperature values of 200 K. (2) Kjergaard *et al.* 1982. (3) Cottrell and Sneden 1985. (4) Kraft *et al.* 1982, Group I stars ([Fe/H] ≥ -2.0) only. (5) Kraft *et al.* 1982, Group II stars ([Fe/H] < -2.0) only. (6) Barbuy 1983. (7) An average of available oxygen abundances for Population II stars; see the compilation of Sneden 1985, and references therein.

warnings in mind when comparing the results of different studies.

Explanations for the abnormally small C/N ratios in very metal-poor giants generally have been variations on two basic ideas: (1) primordial abundance variations in carbon and especially nitrogen in the halo interstellar gas; (2) more extensive mixing and processing, by meridional circulation currents, of the envelopes of the metal-poor giants to the CN-cycle burning layers. A good discussion of the arguments and supporting data for each of these ideas has been given by Langer and Kraft (1984; hereinafter LK84). Those authors showed that the C and N abundances in many Population II giants favor the internal evolution scenario, and they suggested that (for as yet poorly understood reasons) the degree of mixing between the outer envelope and the interior CN-cycle burning region varies greatly from star to star among very metal-poor giants. A recent paper by Norris and Pilachowski (1985), however, finds some good observational evidence to support the assertions of substantial primordial abundance variations. That paper argues that the appearance of sodium enhancements in cluster giants which also are nitrogen-rich cannot easily be explained by mixing effects. Indeed, even the LK84 paper was forced to conclude that, at least for M15 and M92, some primordial abundance variations in [(C + N)/Fe] had to occur along with the mixing, in order to make sense of the C/N ratios in giants of those clusters.

If LK84 are correct in claiming that the envelopes of metal-poor Population II giants contain larger fractions of CN-cycle processed material than do those of Population I giants, then stars which exhibit anomalously low C/N ratios also should possess very low carbon isotope ratios at their surfaces (of course, primordial C and/or N abundance variations could weaken this expected correlation). Recent work on the CNO abundances in Population II stars still on the main sequence suggests that the zero-age C/N ratios for most stars with [Fe/H] ≥ -2 are roughly solar at their surfaces (see Laird 1985, and references contained therein). Data are much fewer for stars with [Fe/H] < -2 , but recent studies of CH in Population II dwarfs (Tomkin, Sneden, and Lambert 1986; Carbon *et al.* 1986, quoted by Kraft 1985) indicate that [C/Fe] ≥ 0 for the most metal deficient main-sequence stars. Therefore since LK84 demonstrate that Population II field giants generally conserve [(C + N)/Fe], and since dwarf stars show C/N ratios of order $\log(C/N) \approx +0.7$, then evolved stars with $\log(C/N) \leq -0.2$ (a factor of 8 decrease in the ratio) ought also to have surface $^{12}\text{C}/^{13}\text{C}$ ratios approaching the CN-cycle equilibrium value of 3.4.

The carbon isotope ratio has been determined only for one extremely metal-poor giant, HD 122563. This well-studied star has the following abundance pattern: (a) [Fe/H] ≈ -2.6 (many analyses; see references in Sneden and Parthasarathy 1983); (b) [C/Fe] ≈ -0.3 and [N/Fe] $\approx +0.7$ (Sneden 1973; Carbon *et al.* 1982; Barbuy 1983); (c) [O/Fe] $\approx +0.6$ (Lambert, Sneden, and Ries 1974); and (d) $^{12}\text{C}/^{13}\text{C} \approx 5$ (Lambert and Sneden 1977). In their discussion of the carbon isotope ratio in HD 122563, Lambert and Sneden (1977) noted that other mildly metal-poor giant stars, such as Arcturus, also exhibit low $^{12}\text{C}/^{13}\text{C}$ values. However, HD 122563 and old disk giants are not drawn from the same stellar population; thus their isotope ratios may not be directly comparable.

Cohen and Grasdalen (1968) attempted to estimate $^{12}\text{C}/^{13}\text{C}$ in a number of metal-poor stars, including HD 122563. However, they concentrated on warmer dwarf stars, and only had low signal-to-noise photographic spectra available for their study. Therefore, they were able to derive only lower limits for this ratio in any of their stars. We recently have obtained high-resolution, high S/N CCD spectra to study the heavy-element abundance patterns in extremely metal-poor giants. These spectra include the region of the CH G band near 4300 Å, and thus prompt our new investigation of the carbon isotope ratio in these halo stars. In the following sections we report and discuss the discovery of very low $^{12}\text{C}/^{13}\text{C}$ ratios in many Population II giants.

II. OBSERVATIONS AND REDUCTIONS

The primary data for this study were obtained on two separate observing runs with the Kitt Peak National Observatory 4 m telescope, Cassegrain echelle spectrograph, and a CCD detector. For each run we employed a 31.6 lines mm^{-1} echelle grating and a suitable cross-disperser grating for the 4300 Å spectral region. For the first set of observations we employed an RCA 320 \times 512 blue-sensitive CCD chip with 30 μm pixel sizes, and for the second set of observations, we switched to a TI 800 \times 800 CCD chip with effective 15 μm pixels. The decision to use the TI chip on the second observing run was dictated by the better S/N characteristics, and by the smaller frequency of radiation events of the TI chips. The projected spectrograph slit width was the same for both sets of spectra, providing effective resolutions of ~ 0.17 Å on all spectra. The S/N values for these spectra varied from ~ 50 for the faintest program stars to ~ 100 for the brighter ones.

Supplemental observations were obtained with the McDonald Observatory 2.7 m telescope and coude spectrograph, with both Digicon (Tull, Choisser, and Snow 1975) and Reticon

(Vogt, Tull, and Kelton 1978) silicon diode array detectors. The McDonald spectra had central wavelengths of 4230 Å or 4370 Å, covered ~ 50 Å at resolutions of 0.13 Å, and had S/N values always exceeding 100. These observations were taken to help define the most useful ^{13}CH features for our analysis, to obtain high S/N spectra of two Population II dwarfs, and to provide higher resolution spectra of the brightest giants.

The reductions of these spectra were accomplished through the use of standard spectrum reduction packages at KPNO and Texas. The initial CCD spectra extractions, including bias subtraction, flat-field corrections, and cosmic ray suppression, were done with software developed at KPNO. The final reductions of all spectra (conversions to wave length scales, fourier transform smoothing, continuum placement, etc.) were performed with the spectrum reduction package written at Texas by Uomoto (1981).

III. SELECTION OF ^{13}CH FEATURES

Inspection of Figure 2 in the Lambert and Sneden (1977) paper illustrates the difficulty in deriving carbon isotope ratios in very weak-lined stars such as HD 122563. The parent ^{12}CH lines useful for isotope ratio studies are no more than 20% deep in that star. Therefore the $^{12}\text{C}/^{13}\text{C}$ values must be quite low simply to be able to detect the ^{13}CH lines. However, one expects values of $^{12}\text{C}/^{13}\text{C}$ never to fall below ~ 3.4 , the CN-cycle equilibrium value; thus the ^{13}CH line depths always will be small in very metal-poor stars. On the other hand, we should stress that HD 122563 is a extreme example. Other halo giants are somewhat more metal rich, and/or are cooler than the 4600 K effective temperature of HD 122563. Both of these effects will strengthen the ^{12}CH features and make the ^{13}CH lines easier to detect at the same isotope ratios. In any case, special care must be used in selecting ^{13}CH features which both are real and lack significant atomic and ^{12}CH contamination. We followed several steps in the selection of appropriate ^{13}CH lines.

The CH $A^2\Pi-X^2\Delta$ system parameter analysis carried out by Krupp (1974), provided the molecular constants for the prediction of wavelengths, excitation potentials, and rotational line strength factors of normal and isotopic lines of the $\Delta v = 0$ sequence near 4300 Å. We adopted the vibrational band oscillator strengths determined by Chmielewski (1984). Only the vibrational bands (0-0), (1-1), and (2-2) are detectable in stars, and only lines with rotational quantum numbers less than ~ 40 are seen, because of the severe predissociation of CH. Moreover, the Q -branch lines of any CH band cannot be employed in a $^{12}\text{C}/^{13}\text{C}$ analysis, since the isotope shifts in this branch are extremely small. Therefore the search for suitable ^{13}CH features was limited to two small spectral regions: 4215-4250 Å for R -branch lines, and 4345-4380 Å for P -branch lines.

We first used the solar spectrum to predict useful ^{13}CH lines (see similar discussions by Sneden 1983; Lambert and Sneden 1977). Predictions of the strengths of ^{13}CH features in the Sun were made with a standard line analysis program (Sneden 1973), the solar atmosphere model of Holweger and Muller (1974), the CH molecular parameters, the solar C and O abundances derived by Lambert (1978), and an assumed solar isotope ratio of $^{12}\text{C}/^{13}\text{C} = 89$. Then, solar lines likely to have significant contributions by ^{13}CH were selected through inspection of the Liège solar atlas (Delbouille, Neven, and Roland 1973) and the solar line identifications of Moore, Minnaert, and Houtgast (1966). We measured the equivalent width

TABLE 2
 ^{13}CH LINE DATA

Wavelength (Å)	ID(^{13}CH)	EW_0 (mÅ)	ID(atomic)	EW_{star} (mÅ)
4221.80.....	(0-0) $R_{1,cd}(21)$	0.6	Fe II	0.1
4230.30.....	(0-0) $R_{1,2dc}(15)$	12.5	Cr I	0.9
4231.45.....	(0-0) $R_{1,2dc}(13)$	1.4	Ti I	0.8
4236.55.....	(0-0) $R_{1,2cd}(12)$	1.5	Zr I	0.5
			Zr II	0.8
4237.55.....	(0-0) $R_{1,2dc}(12)$	4.1	Ti I	1.1
			Sm II	0.5
4359.1.....	(1,1) $P_{1,2dc}(10)$; (0,0) $P_{2cd}(10)$...	Blend	≈ 1.5
4360.0.....	(0,0) $P_{1,2dc}(10)$	5.7	Cr I	0.7
			Fe II	0.3
4363.9.....	(0-0) $P_{1,2dc}(11)$	0.5
4366.18.....	(0-0) $P_{2dc}(12)$	0.5
	(1-1) $P_{1cd}(12)$			
4370.70.....	(0-0) $P_{1,2dc}(13)$	3.9	Cr I	0.2
			Os I	1.5

of each probable ^{13}CH line, and in Table 2 we list these features and their solar equivalent widths.

Identification of other transitions which could contribute to the total absorption of the ^{13}CH features was accomplished with the aid of the line lists of Kurucz and Peytremann (1975), Meggers, Corliss, and Scribner (1975), and Moore *et al.* (1966). To assess the probable amount of contamination of each ^{13}CH line by these other species, we first derived upper limits for the "solar" oscillator strengths for the possible atomic contaminants, with the assumption that each of these transitions provided the total equivalent width of the given line. Finally, the equivalent width of each contaminant was determined for a typical program star, HD 110184, which has been studied previously by Luck and Bond (1981) and by Sneden and Pilachowski (1985). For this task we adopted the model atmosphere derived by Sneden and Pilachowski, ($T_{\text{eff}}/\log g/[Fe/H]/v_{\text{micro}} = (4500/0.85/-2.3/3.0 \text{ km s}^{-1})$) and used the same line analysis program described previously. As expected, most potential contaminating atomic transitions proved to be vanishingly weak in the very metal deficient star, especially lines of neutral species, or lines with high-excitation potential (> 1 eV). In Table 2 we give the identification and predicted metal-poor star equivalent width of any significant atomic contaminant transition. Since our method of determining the oscillator strengths of the contaminant lines yielded overestimates for their gf -values, the contributions of these transitions should actually be less than indicated in Table 2. However, we must caution that the line lists consulted for this test leave a considerable fraction of all solar features unidentified, and it is possible that unknown contaminants still may lurk in our final set of ^{13}CH lines.

The next test for acceptable ^{13}CH lines was the synthesis of the CH spectrum of stars with well-known carbon isotope ratios. We chose μ Aql and α Boo for this task, because they are K giants with very different values of $^{12}\text{C}/^{13}\text{C}$, as derived from analyses of CN red system lines: 44 for μ Aql (Lambert and Ries 1981) and 7.2 for α Boo (Lambert and Dearborn 1972; Day, Lambert, and Sneden 1973). In Figure 1 we show part of the CH spectra of these two stars. Obvious differences exist between the absorption strengths of the indicated ^{13}CH features. With appropriate model atmospheres, and line lists generated with and without atomic transitions, we synthesized the CH spectra for both stars and compared these with the observed spectra. The total abundance of carbon was permit-

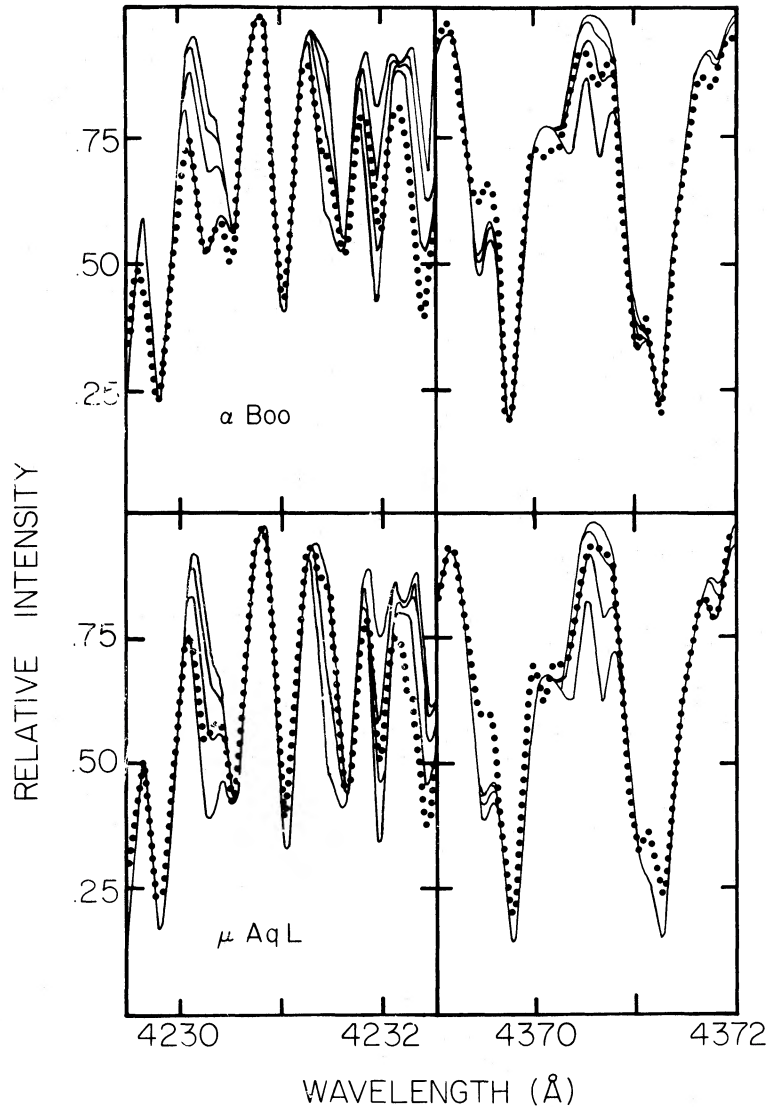


FIG. 1.—Part of the CH spectra of μ Aql and α Boo. Dotted curves are the observed spectra, and solid curves are the synthetic spectra. Both atomic and molecular lines have been included in the syntheses. The abundance of ^{12}CH was permitted to be a free parameter to match the observed ^{12}CH line depths for each star, and spectra were computed for isotope ratios of $^{12}\text{C}/^{13}\text{C} = 3, 9, 27,$ and 81 .

ted to be a free parameter to match the observed ^{12}CH line depths, since only isotope ratios were desired here. In Figure 1 we show these syntheses, and in Table 3 we give estimates of the $^{12}\text{C}/^{13}\text{C}$ ratio in these stars from each ^{13}CH feature. Reasonable agreements with the published isotope ratios for μ Aql and α Boo were achieved, confirming the sensitivity of the chosen lines for our analysis.

Note from the entries in Table 3 that some of our chosen ^{13}CH lines could not be used in the analysis of μ Aql and α Boo, for the atomic line blending is very severe in the 4300 Å spectra of these cool giants. However, these metal-rich stars present greater blending problems than do the very metal-poor program stars. Obviously, the atomic line opacities decrease by factors of tens to thousands from μ Aql and α Boo to typical Population II giants, but the CH line strengths do not drop as quickly. Metal-poor giants have lower continuous opacities and hence higher gas pressures and lower electron pressures than do metal-rich stars of similar T_{eff} and $\log g$ values. Taken together, these atmosphere structure effects increase the line

opacities of CH in comparison with those of neutral and ionized atomic lines. Single slab curve-of-growth arguments which predict these relationships may be seen in, for example, Pagel (1964).

Sample line calculations using the Bell *et al.* (1976) grid of model atmospheres provided quantitative confirmation that line strengths of CH weaken more slowly than do those of atomic lines in very metal-poor stars. For example, we considered two model atmospheres with $T_{\text{eff}} = 4500$ K and $\log g = 1.5$, but differing in metallicity: $[\text{M}/\text{H}] = 0$ and -2 . In the line-forming regions of these atmospheres, the gas pressures in the metal-poor atmosphere are ~ 0.8 dex higher than those of the metal-rich model, the electron pressures are ~ 0.8 dex lower, and the temperatures are about equal. For elements which are easily ionized, the abundance of that element necessary to produce a line of given equivalent width changed by only 0.01 dex for neutral species between the metal-rich and metal-poor models. Therefore neutral-line strengths do not depend on the gas and electron pressure changes which accom-

TABLE 3
 $^{12}\text{C}/^{13}\text{C}$ FROM INDIVIDUAL ^{13}CH FEATURES

STAR	WAVELENGTH/WEIGHT									
	4221.8 1	4230.3 1	4231.4 2	4236.5 2	4237.6 1	4359.1 1	4360.0 1	4363.9 1	4366.2 2	4370.7 2
Standard K giants:										
α Boo	6	...	6	10	8	9	12
μ Aql	30	...	>30	>25	>40	>30	30
Metal-poor dwarfs:										
Gmb 1830	>20	15	>50	>50	>30	10?	30	>50	>50	50
HD 140283	>10	10	>20	>10	>20	>10	>10	>10	10	>10
Metal-poor giants:										
HD 63791	10:	6	10	7		6	9	10	8	8
HD 83212	3	3	7:	3	3	3:	5	10	6	5
HD 88609	10:	10:	5:	8	5:	10:	4	10	15:
HD 108317	>30	15	>30	30:	10	>30	20:	>30	>10	10
HD 110184	3	3	3	2	3	3	5	4	4	5
HD 115444	3:	3	10	10:	6	3	3	3	8	7
HD 122563	2	2.5	5	4	3	3	8:	9:	4	3
HD 122956	5	5	7	5	4	4	6	7	6	6
HD 126587	8	15:	30	10	10	15	30	10	20:	10
HD 128279	30:	25:	>30	>20	30	>30	30	>30	20	>25
HD 175305	>50	20	>30	50	20:	10	30	>50	50	30
HD 165195	2	2	7	>4	3	4:	4	7	4	5
HD 221170	3	3.5	2	7	4	5?	10	10	5	6
+58° 1218	3	8	20:	>30	10?	10?	>30:	7:	10:	20:
-18° 5550	10:	15:	30:	20:	10:	10:	>30	15:	15:	>30

pany metallicity changes. For ionized lines, abundances of ~ 0.5 dex less were needed in the metal-poor atmosphere to yield the same line strengths seen in the metal-rich atmosphere, as a result of the drop in electron pressures; thus ionized lines remain stronger than neutral lines in metal-poor stars. Finally, the increase in gas pressures in the metal-poor star strengthened the CH lines: carbon abundances of ~ 1 dex smaller in the metal-poor atmosphere resulted in the same CH equivalent widths obtained in the metal-rich case. Precise specification of the increase in strength of CH lines in metal-poor stellar atmospheres depends on some molecular equilibrium details involving the abundance of oxygen in the star, but the implication is very clear: CH lines weaken much less rapidly than atomic lines in the spectra of metal-poor stars. ^{13}CH features which were unusable in stars such as μ Aql provided valuable carbon isotope ratio information in the program giants.

For a last check of the utility of our chosen ^{13}CH lines, we rederived the $^{12}\text{C}/^{13}\text{C}$ ratio for HD 122563 from both the KPNO and McDonald spectra. These data sets are of lower resolution than that employed in the Lambert and Sneden (1977) study (0.08 Å), and consequently the line-blending problems are more severe. The new determinations confirmed the earlier value of $^{12}\text{C}/^{13}\text{C} \approx 5$ in that star (see Table 3).

From the synthesis of the spectra of all these stars we chose primary and secondary ^{13}CH features for our analysis. Our estimate of the reliability of each line is given in Table 3. A weight of 2 was assigned to those features which yielded isotope ratios which were in good agreement with the published ratios for the standard stars. We gave a weight of 1 to the features which exhibited some sensitivity to the isotope ratio, but clearly had some extra (and often unidentified) atomic absorption present. Five of these lines have been employed in other stellar carbon isotope ratio investigations. Lambert and Mallia (1968) suggested that the 4231.4 Å (0-0) $R_{1,2dc}(13)$ doublet is the cleanest ^{13}CH feature in the solar

spectrum. A new study underway by Chmielewski and Lambert (private communication) adds the 4370.7 Å (0-0) $P_{1,2dc}(13)$ doublet, and perhaps the 4363.85 Å (0-0) $P_{1dc}(11)$ line, as useful transitions for the derivation of the solar $^{12}\text{C}/^{13}\text{C}$ value. Finally, the original CH study of α Boo by Lambert and Dearborn (1972) employed the 4370.7 Å feature as one of their primary ^{13}CH strength measures, and also used the 4363.85 Å and 4359.97 (0-0) $P_{2dc}(10)$ lines as secondary features, although they noted that in Arcturus the latter two lines are blended. The other features used in our study are too contaminated in such strong lined stars as the Sun and α Boo.

IV. DERIVATION OF CARBON ISOTOPE RATIOS

a) Atmosphere Parameters

Model atmosphere parameters for most program stars were computed from the data given by K82. For temperatures, we used the averages of their $B-V$ and $V-R$ effective temperature estimates. Gravities were interpolated from the values shown in Figure 9 of Carbon *et al.* (1982), which provided a conversion from the observed $(B-V)_0$, V_0 photometry of the stars (Bond 1980) to T_{eff} , $\log g$ values. This conversion assumed that the field Population II giants possess the same giant branch parameters as the very metal-poor globular cluster M92 ($[M/H] \approx 2.3$; Cohen 1979); thus absolute magnitudes M_v and gravities could be obtained directly from knowledge of $(B-V)_0$. Metallicity values were taken directly from K82. The program stars HD 83212, HD 126587, and HD 128279 were not observed in the K82 survey. For HD 83212 and HD 126587, we used the Bond (1980) values of $(B-V)_0$ and V_0 to obtain T_{eff} , $\log g$ estimates in the manner described above. For HD 128279, we adopted the parameters derived by Barbuy (1981). The models for HD 122563 and HD 110184 were taken from Sneden and Pilachowski (1985).

All of the adopted model atmosphere parameters are listed

TABLE 4
 STELLAR QUANTITIES

Star	M_v	T_{eff}	$\log g$	[Fe/H]	v_{micro}	[C/Fe]	[N/Fe]	$\log(\text{C/N})$	$^{12}\text{C}/^{13}\text{C}$
Standard K giants:									
α Boo ^a	+0.3	4350	1.5	-0.7	1.8	-0.4	+0.0	+0.3	8
μ Aql ^a	+2.1	4500	2.0	+0.0	2.0	-0.1	+0.2	-0.3	44
Metal-poor dwarfs:									
Gmb 1830 ^b	5000	4.6	-1.4	1.0	-0.5	-0.5	+0.7	>50
HD 140283 ^b	5600	4.5	-2.3	1.0	-0.2	-0.5	+1.0	>10
Metal-poor giants:									
HD 63791	-0.6	4750	1.8	-1.8		-0.4	+0.0	+0.3	8
HD 83212	-0.5	4800	2.0	-1.5:					5
HD 88609	-1.5	4600	1.3	-2.6	3.2 ^c , 2.0 ^d	-1.0	+0.4	-0.7	10:
HD 108317	+1.3	5125	2.6	-2.3	1.5 ^e	-0.4	-0.2	+0.5	>25
HD 110184	-2.3	4500	0.85	-2.3	2.7 ^c , 3.0 ^e	-1.0	+0.2	-0.5	3.5
HD 115444	-1.1	4750	1.6	-2.7	2.6 ^f	-0.4	+0.4	-0.1	7
HD 122563	-1.5	4600	1.2	-2.7	2.8 ^c , 1.8 ^g , 2.3 ^c	-0.5	+0.5	-0.3	4
DH 122956	-0.9	4600	1.1	-1.9		-0.4	+0.1	+0.2	6
HD 126587	-1.0	4750	1.1	-2.7	2.0 ^c	17
HD 128279	+0.9	5050	2.5	-2.5	1.0 ^g	+0.15 ^h	+0.5 ^h	+0.35 ^h	>30
HD 165195	-1.8	4500	1.1	-2.2		-1.0	-0.1	-0.2	4.5
HD 175305	+1.2	5200	2.7	-1.5		40
HD 221170	-1.9	4500	1.1	-2.4		-0.3	+0.3	+0.1	6
+58° 1218	-0.2	4950	2.1	-2.6	2.2 ^c	-0.3	-0.5:	+0.9:	17
-18° 5550	-1.4	4560	1.3	-3.5	2.9 ^c	21

^a All quantities are from Lambert and Ries 1981, adjusted to a lower temperature scale.

^b All stellar quantities are from Tomkin and Lambert 1984.

^c Luck and Bond 1985.

^d Snenen 1974.

^e Snenen and Pilachowski 1985.

^f Griffin *et al.* 1982.

^g Barbuy 1981.

^h Barbuy 1983.

in Table 4. We computed model atmospheres with these parameters, using the giant star atmosphere grid of Bell *et al.* (1976), and interpolation routines written by P. L. Cottrell (private communication).

The final atmosphere parameter to be specified was the microturbulent velocity. Many of our program stars have not been subjected to the high-resolution analyses necessary to evaluate this parameter. In Table 4 we have gathered previous estimates of the microturbulence for our stars; the average value is $v_{\text{micro}} = 2.2 \pm 0.2 \text{ km s}^{-1}$. Notice, however, the rather large range in claimed microturbulent velocities in otherwise similar metal-poor giants. Moreover, the uncertainties quoted in the various papers for each v_{micro} value typically are $\pm 0.5 \text{ km s}^{-1}$. Therefore, for this survey, we adopted $v_{\text{micro}} = 2.0 \text{ km s}^{-1}$ for all stars. This value deliberately was chosen to be on the low side of the microturbulence estimates. Only the ^{12}CH lines are strong enough to experience saturation effects in the program stars. Therefore, if we have underestimated the microturbulence in any star, we will have overestimated the abundance of ^{12}C ; thus it follows that our $^{12}\text{C}/^{13}\text{C}$ estimates are most likely to *decrease*, on average, if our microturbulence values are in error. Finally, we note the careful study of Gustafsson, Kjergaard, and Andersen (1974) of microturbulence in Population I K giant stars, which concluded that $\langle v_{\text{micro}} \rangle \approx 1.7 \text{ km s}^{-1}$. This provides some mild support for our choice of 2 km s^{-1} for our stars. Further comments on microturbulence are given in § IVd of this section.

b) $^{12}\text{C}/^{13}\text{C}$ in Metal-poor Dwarfs

We attempted to derive carbon isotope ratios in two well-known Population II dwarf stars, Gmb 1830 and HD 140283,

in order to determine likely primordial $^{12}\text{C}/^{13}\text{C}$ values for the metal-poor giant stars. Tomkin and Lambert (1984) derived C and N abundances for both of these stars, and we adopted the model atmosphere parameters recommended by them. In Figure 2 we show observed and synthetic spectra for Gmb 1830. The ^{13}CH could not be detected with certainty in either star, and therefore we have derived only lower limits to the $^{12}\text{C}/^{13}\text{C}$ values. Naturally, since the ^{12}CH lines are much stronger in Gmb 1830 than in HD 140283, a larger lower limit may be placed on its isotope ratio. In fact, the ^{12}CH lines in the HD 140283 spectrum are too weak to be able to place really meaningful limits on its isotope ratio, given the resolution and signal-to-noise of our spectra. The line-by-line isotope ratio estimates for both stars appear in Table 3, and final isotope ratio limits are given in Table 4. The $^{12}\text{C}/^{13}\text{C}$ entries were calculated using all features, but giving double weight to the primary ^{13}CH features.

The limits of $^{12}\text{C}/^{13}\text{C}$ in these very metal-poor dwarfs indicate that any low values of $^{12}\text{C}/^{13}\text{C}$ seen in metal-poor giants are caused by the internal evolutions of those stars. Clearly, we also affirm the basic conclusion of Cohen and Grasdalen (1968). That is, if (a) the Galaxy began with a first generation of supermassive stellar objects, and (b) if these objects synthesized large amounts of ^{13}C (Wagoner, Fowler, and Hoyle 1967), then at least one other generation of ordinary massive stars (which produce large amounts of ^{12}C ; see, e.g., Arnett 1978) must have existed before the formation of the present Population II stars.

The pursuit of accurate $^{12}\text{C}/^{13}\text{C}$ ratios in Population II dwarf stars should be continued in the future to clear up remaining uncertainties in the initial values of this ratio in metal-poor stars. HD 140283 should be reobserved at higher

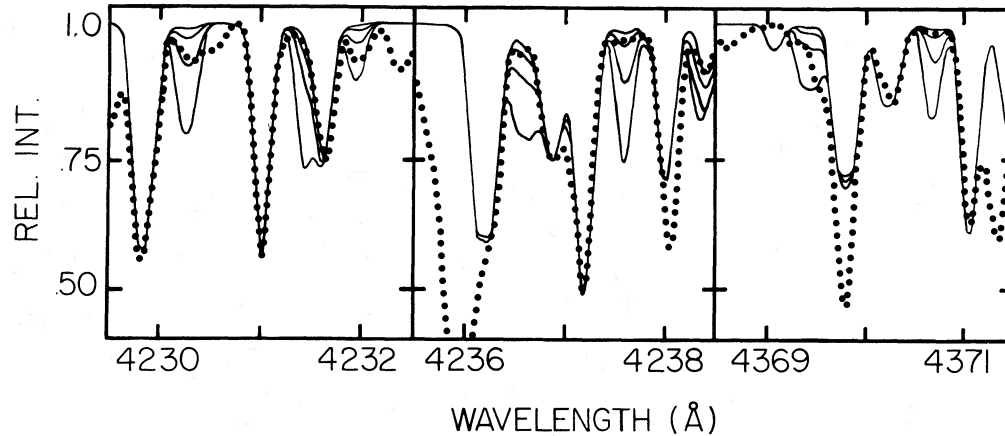


FIG. 2.—Part of the CH spectra of the metal-poor dwarf star Gmb 1830 (HD 103095). Dotted and solid curves are as in Fig. 1. We have not included any atomic transitions in these syntheses, in order to show clearly the positions and strengths of the ^{12}C and ^{13}C features. The carbon isotope ratios for the syntheses again are 3, 9, 27, and 81, and the ^{12}C abundances are free parameters of fit.

resolution, say 0.05 Å. More importantly, some effort should be made to derive this ratio from the CH spectra of dwarfs with low metallicity, but cooler temperatures, and therefore probably much stronger CH bands than exist in HD 140283. A list of some fairly bright subdwarf stars may be found in Carney (1979*b*). From this compilation, and the $\delta(U-B)_{0.6}$ versus $[\text{Fe}/\text{H}]$ relation of Carney (1979*a*), one can identify such stars as BD + 66°268 and HD 101063 as likely candidates for future work on the carbon isotope ratio in extremely metal-poor dwarfs.

c) $^{12}\text{C}/^{13}\text{C}$ in Metal-poor Giants

We used the identical procedures described above to derive estimates of the $^{12}\text{C}/^{13}\text{C}$ ratio in the program giants. Many of our giants exhibit very low carbon isotope ratios. Examples of the synthetic and observed spectra which illustrate this point appear in Figure 3, the single feature isotope ratio estimates are given in Table 3, and final average values are in Table 4. As before, the total carbon abundance of a star was permitted to be a free parameter. The oxygen abundance was defined arbitrarily as $[\text{O}/\text{H}] = [\text{Fe}/\text{H}] + 0.5$. However, K82 emphasize that in extremely metal deficient giants, the formation of CO is not too severe for stars with $T_{\text{eff}} > 4250$ K or so; thus, knowledge of the O abundances are not critical for our computations. It is worth noting that our resulting C abundances correlate extremely well with those of K82: $[\text{C}/\text{Fe}]_{\text{this study}} - [\text{C}/\text{Fe}]_{\text{K82}} \approx -0.05$, and for no star is the difference greater than ± 0.2 .

In § V we discuss the correlations of our isotope ratios with other stellar quantities. However, a simple inspection of our spectra suggests that the strengths of the ^{13}C features seem to increase as the metal-line strengths grow. This does not mean that we have simply misattributed atomic features to ^{13}C , for the effect is mainly a temperature one. Again turning to the lessons of single-slab coarse analyses, it is apparent that the line strengths of atomic and molecular lines scale roughly as $5040/T$ times the excitation potential of the transitions. When this effect is subtracted away, much of the atomic line-molecular line correlation disappears. The ^{13}C line strengths vary by up to factors of 10 for given (temperature corrected) atomic line strengths.

d) Uncertainties in the Isotope Ratios

Any discussion of model atmosphere selection for a carbon isotope ratio study must begin with a statement stressing the insensitivity of $^{12}\text{C}/^{13}\text{C}$ to uncertainties in T_{eff} , $\log g$, and $[\text{Fe}/\text{H}]$. With the total carbon abundance allowed to vary to match the synthetic and observed ^{12}C line depths, small changes in these model parameters will not alter the ratio of the strengths of the ^{12}C and ^{13}C features. No elaborate error analysis for these parameters is necessary here.

However, as indicated in § IVa of this section, the $^{12}\text{C}/^{13}\text{C}$ results must be somewhat sensitive to microturbulence choices because the ^{12}C lines are strong enough in some program stars to experience saturation effects. We have quantified this effect by tabulating in Table 5 the changes in the derived carbon isotope ratio with different assumptions about the values of v_{micro} . For this test we chose two stars: HD 122563, which has very weak ^{12}C features, and HD 165195, a star with much stronger ^{12}C lines. Obviously, microturbulence uncertainty effects play a greater role in the $^{12}\text{C}/^{13}\text{C}$ determination for HD 165195.

However, the entries in Table 5 reemphasize the reasons for our choice of the relatively low value of 2 km s^{-1} for a standard microturbulent velocity. If metal-poor giants possess, in reality, substantially larger v_{micro} parameters (see Table 4), then two effects occur. First, the $^{12}\text{C}/^{13}\text{C}$ values will decrease further. This cannot alter our basic conclusion that very low carbon isotope ratios exist in many metal deficient giant stars. Second, the $^{12}\text{C}/^{13}\text{C}$ ratios quickly approach asymptotic limits as the microturbulence increases, for the ^{12}C lines never are extremely deep in very metal-poor giants, and thus become quite unsaturated for $v_{\text{micro}} > 3 \text{ km s}^{-1}$. Therefore, the isotope

TABLE 5
 $^{12}\text{C}/^{13}\text{C}$ RATIO DEPENDENCES ON MICROTURBULENCE

v_{micro} (km s^{-1})	$^{12}\text{C}/^{13}\text{C}_{\text{HD 122563}}$ $\log(W/\lambda)_{12\text{CH}} \approx -5.25$	$^{12}\text{C}/^{13}\text{C}_{\text{HD 165195}}$ $\log(W/\lambda)_{12\text{CH}} \approx -4.90$
1.....	4.20	5.30
2.....	4.00	4.50
3.....	3.80	3.75
4.....	3.75	3.55

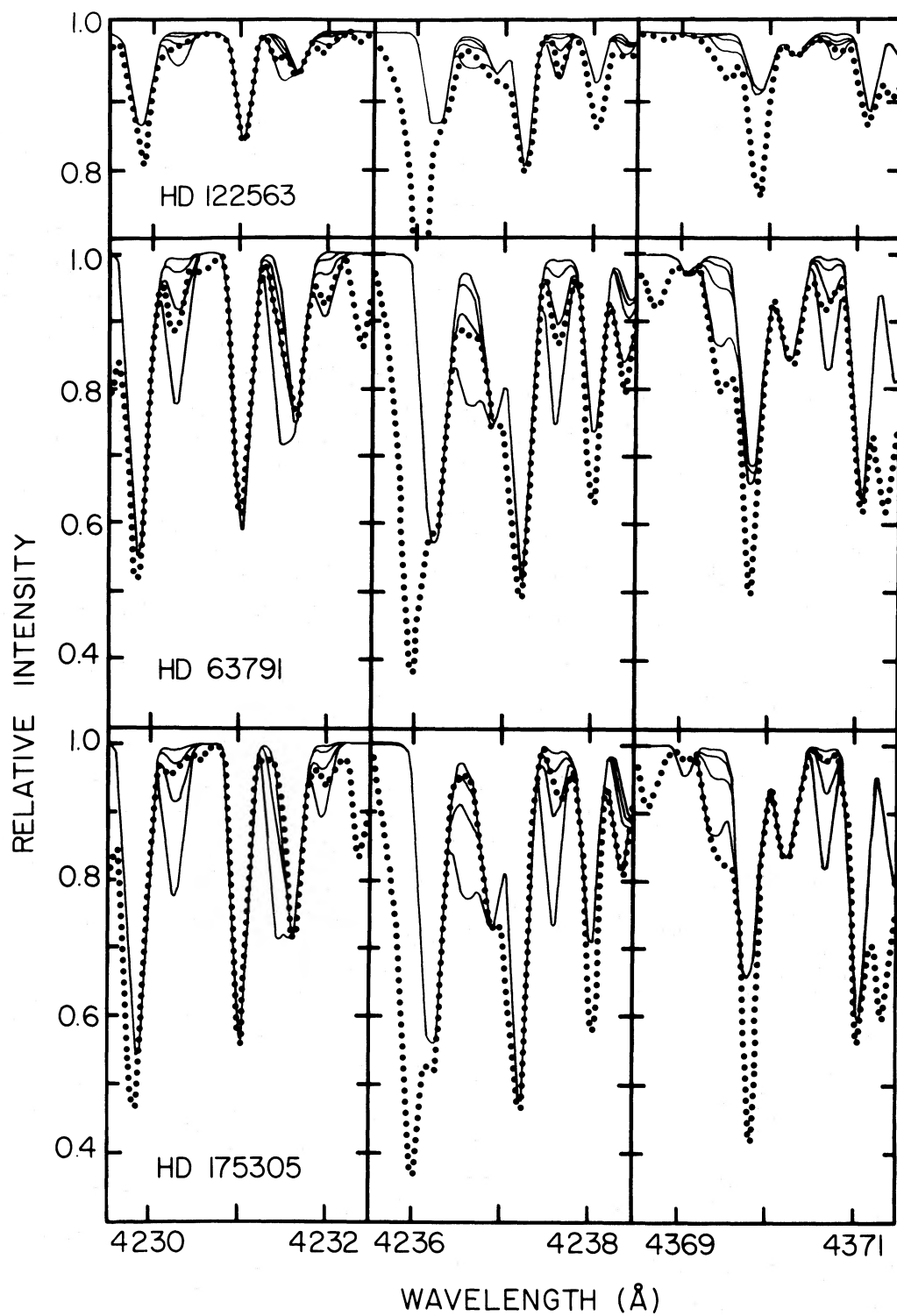


FIG. 3.—Examples of observed (*dotted curve*) and synthetic (*solid curve*) spectra of some of the metal-poor giant stars. The synthesis assumptions are identical to those given in Fig. 2.

ratios would not be altered substantially from their present values if the microturbulence values were to be increased.

V. THE CARBON ISOTOPE RATIO AND THE EVOLUTION OF LOW-MASS, METAL-POOR GIANT STARS

This study has demonstrated that the carbon isotope ratios of extreme Population II field giants are often quite low, and that the large ^{13}C fractions probably are due mainly to the internal evolutions of these stars. Clearly, the discovery of low $^{12}\text{C}/^{13}\text{C}$ values in metal-poor giant stars lends support to the contention of LK84 that large-scale dredge-ups of CN-cycle products have occurred in the envelopes of Population II giants. This conclusion, of course, still does not exclude the possibility that primordial abundance variations produced some (possibly substantial) part of the observed C/N anomalies in metal-poor giants (see § I). Nonetheless, in this section we will limit our discussion to evolutionary processes which could produce the observed carbon isotope ratios and other chemical peculiarities in such stars.

a) Observed Abundance Trends

In Figure 4 we show the correlations of $^{12}\text{C}/^{13}\text{C}$ with effective temperatures and absolute visual magnitudes for the program giants. These fundamental H-R diagram quantities represent the degree of evolution of stars up the giant branch. Since the very metal-poor giants also are kinematically old

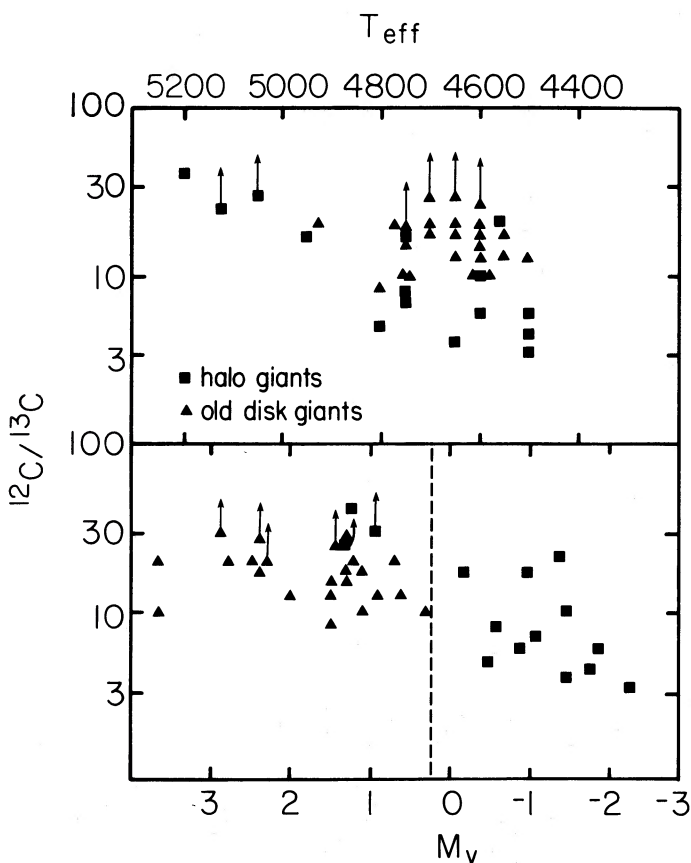


FIG. 4.—Carbon isotope ratios plotted against effective temperatures and absolute visual magnitudes for metal-poor giants. The halo giants are those analyzed in this study, and the points for the old disk giants were taken from Cottrell and Sneden (1985). Dashed line at $M_v = +0.5$ indicates the approximate luminosity for first dredge-up completion.

stars, they share a narrow range of masses near $0.8 M_{\odot}$, and follow nearly identical evolutionary tracks. We also have included in Figure 4 the old disk giants of Cottrell and Sneden (1986), which are kinematically younger. The Cottrell and Sneden stars must be slightly more massive and occupy a wider range of masses, between 0.8 and $1.2 M_{\odot}$. Those stars vary in metal abundance between -0.2 and -0.8 , according to Cottrell and Sneden. The M_v values for the old disk giants have been taken from Wilson (1976).

For the very metal-poor giants of the present study, the carbon isotope ratios appear to be functions of giant branch position: the ratios decline with increasing luminosity and decreasing temperature. In particular, the most luminous Population II giants generally show $^{12}\text{C}/^{13}\text{C} < 20$, with a dominant component having isotope ratios not far from the CN cycle equilibrium value. The old disk mildly metal-poor giants plotted in Figure 4 do not appear to possess such low $^{12}\text{C}/^{13}\text{C}$ values, but ratios still are lower than those predicted from standard theory (see Cottrell and Sneden 1985).

Two additional figures are shown here to aid the interpretation of the carbon isotope ratio results. In Figure 5 we have plotted the correlation of the carbon abundances in extreme Population II stars with absolute magnitude, including in this figure all of the K82 stars and also the extreme Population II dwarfs studied by Tomkin, Sneden, and Lambert (1986). Note in Figure 5 that the $[\text{C}/\text{Fe}]$ values for the dwarf stars exhibit a large (± 0.3 dex) range. Part of this scatter may be due to a trend of increasing $[\text{C}/\text{Fe}]$ with decreasing $[\text{Fe}/\text{H}]$; see Tomkin *et al.* However, for the giants, most of the stars with extremely low $[\text{C}/\text{Fe}]$ values are the most metal-poor (this point is shown in the K82 and K84 papers). Again, the amount of CN cycle processing seen at the surface of a giant appears to be inversely correlated with overall stellar metallicity.

In Figure 6 we compare the carbon abundances with the $^{12}\text{C}/^{13}\text{C}$ ratios for both the Population II giants of the present study and the old disk giants of the Cottrell and Sneden (1986) survey. The data of Figure 6 demonstrate that the extreme Population II giants show a large spread in the surface carbon abundances for the same carbon isotope ratios. This stands in sharp contrast to the sample of old disk giants, which exhibit a narrower range of carbon isotope ratios and carbon abundances ($^{12}\text{C}/^{13}\text{C} \approx 10$ to 20 , $[\text{C}/\text{Fe}] \approx -0.1 \pm 0.15$), and a narrower range of M_v . All of the extreme Population II giants which have low values of $^{12}\text{C}/^{13}\text{C}$ are very luminous stars. It is apparent that these stars have processed nearly their entire envelopes through at least a partial CN cycle, enough to bring the surface carbon isotope ratios near to the CN-cycle equilibrium values. Presumably, the large variations in $[\text{C}/\text{Fe}]$ which accompany the low $^{12}\text{C}/^{13}\text{C}$ values must tell us something about the depths of the convective envelope and/or the interior temperatures of these stars.

b) Predicted Abundance Trends

Two theoretical processes commonly are invoked to explain the variations in surface abundances and isotope ratios of the CNO elements in low-mass stars which are evolving up the red giant branch. The first process is the standard "first dredge-up" (e.g., see Iben and Renzini 1984), and the second process, called "meridional mixing," has been proposed by Sweigart and Mengel (1979) to explain anomalous CNO abundances in both Population I and II giants. Surface abundances can be altered as the convective envelope of a red giant star dips into the interior of the star to mix with material which has under-

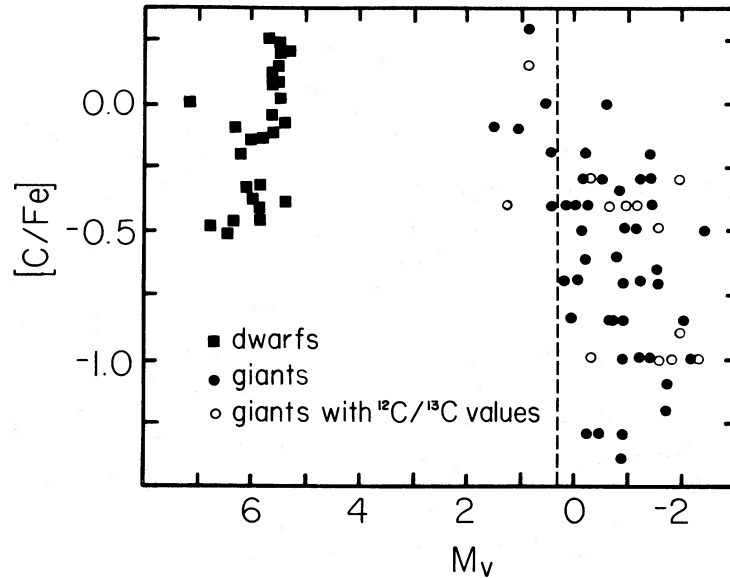


FIG. 5.—Carbon abundances as functions of absolute visual magnitudes for very metal-poor stars. Dwarf star data were taken from Tomkin *et al.* (1985), and the giant star points were adopted from the extensive K82 study. Again, the dashed line shows the first dredge-up completion luminosity.

gone CN-cycle processing during its main-sequence evolution. According to Iben and Renzini, in low-mass, solar composition stars, the first dredge-up is expected to decrease the abundance of carbon by 30% (i.e., $[C/Fe]$ drops by 0.15 dex), decrease the $^{12}C/^{13}C$ ratio from ~ 90 to 20–30, and decrease $\log(C/N)$ by ~ 0.4 dex. The effects of this dredge-up should be complete by the time that a star reaches a luminosity of $M_v \approx +1.4$.

However, the first dredge-up works with decreased efficiency in giants of the same mass, but of smaller metal abundances (or in those having the same metallicity but lower masses). In a recent computation of 34 red giant branches (RGBs) for low-mass stars with $-2.3 \leq [Fe/H] \leq -0.5$, Vandenberg (1986, hereinafter V86) has predicted the surface abundances of the CNO elements at the point in each evolutionary track where the mass contained in the convective envelope reaches a maximum. A representative sample of the carbon isotope

ratios and the $\log(C/N)$ values found in these model calculations is provided in Table 6. The entries of this table show clearly that the classical first dredge-up cannot account for the isotope ratios of most of our program giants. For all reasonable assumptions about the stellar masses of extreme Population II stars ($M < 0.9 M_{\odot}$), the isotope ratios remain large: $^{12}C/^{13}C > 30$ (obviously, the overall carbon and nitrogen abundances at the surface also are altered very little). A similar conclusion has been reached independently by R. T. Rood (private communication) from consideration of the evolution of ^{12}C abundances in globular cluster red giant models.

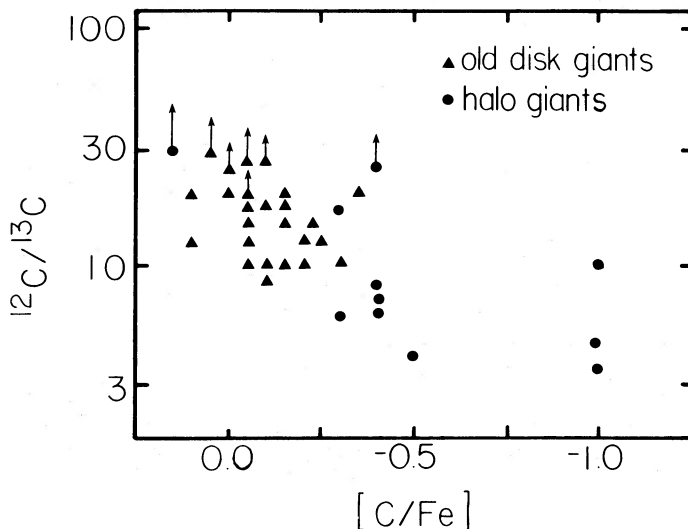


FIG. 6.—Carbon isotope ratios vs. carbon abundances for the very metal-poor giants and the old disk giants. Data sources are as in Fig. 4.

TABLE 6
CARBON ISOTOPE AND C/N RATIOS FROM FIRST DREDGE-UP

Z	Y	M	M_{env}^a	M_{bol}^b	M_{bol}^c	$^{12}C/^{13}C$	$\log(C/N)$
0.0001	0.2	0.8	0.352	+0.45	-0.70	67	0.67
		0.9	0.359	+0.15	-0.85	34	0.62
		1.0	0.365	-0.10	-1.10	29	0.49
0.0001	0.3	0.7	0.353	+0.35	-0.80	77	0.68
		0.8	0.362	-0.05	-1.05	36	0.64
		0.9	0.370	-0.35	-1.35	28	0.49
0.0003	0.2	0.8	0.329	+0.65	-0.35	58	0.67
		0.9	0.336	+0.35	-0.65	32	0.60
		1.0	0.342	+0.10	-0.80	28	0.47
0.0003	0.3	0.7	0.331	+0.55	-0.55	69	0.67
		0.8	0.339	+0.20	-0.85	32	0.62
		0.9	0.347	-0.15	-1.10	28	0.48
0.001	0.2	0.8	0.302	+1.10	+0.05	50	0.67
		0.9	0.307	+0.75	-0.15	32	0.59
		1.0	0.313	+0.55	-0.35	28	0.47
0.001	0.3	0.7	0.304	+1.00	-0.15	61	0.67
		0.8	0.311	+0.60	-0.40	33	0.60
		0.9	0.319	+0.35	-0.70	28	0.48

^a Mass (in solar units) interior to the inner boundary of the convective envelope at maximum penetration.

^b Luminosity of maximum penetration of the convective envelope.

^c Luminosity at which the H-burning shell first contacts the composition discontinuity produced during the first dredge-up.

Before explaining why the efficiency of the first dredge-up is such a sensitive function of both mass and metallicity, it is instructive to review the nucleosynthesis of the CNO elements in a typical low-mass Population II star (Dearborn, Eggleton, and Schramm 1976 provide a complementary analysis of Population I stars). For our example, we will consider the case of a $0.8 M_{\odot}$ star having $Y = 0.2$ and $Z = 10^{-4}$ for the initial mass-fraction abundances of helium and the heavier elements, respectively. The evolutionary track of such a model star is shown in Figure 7, where the segment from the zero-age main sequence to the base of the RGB is tabulated by Vandenberg and Bell (1985), while its continuation to the helium flash point is given by V86. The latter study is also the source of the RGB for the $1.0 M_{\odot}$ model with the same initial chemical composition: it has been plotted in Figure 7 to illustrate the sensitivity of the location of the RGB in the $(M_v, \log T_{\text{eff}})$ plane to the total stellar mass. Vandenberg (1984) already has demonstrated that these models (for $[\text{Fe}/\text{H}] = -2.3$) provide an excellent match to the H-R diagram locations of M92 giants. Therefore, it is not surprising that there is equally fine agreement between the same models and the sample of extremely

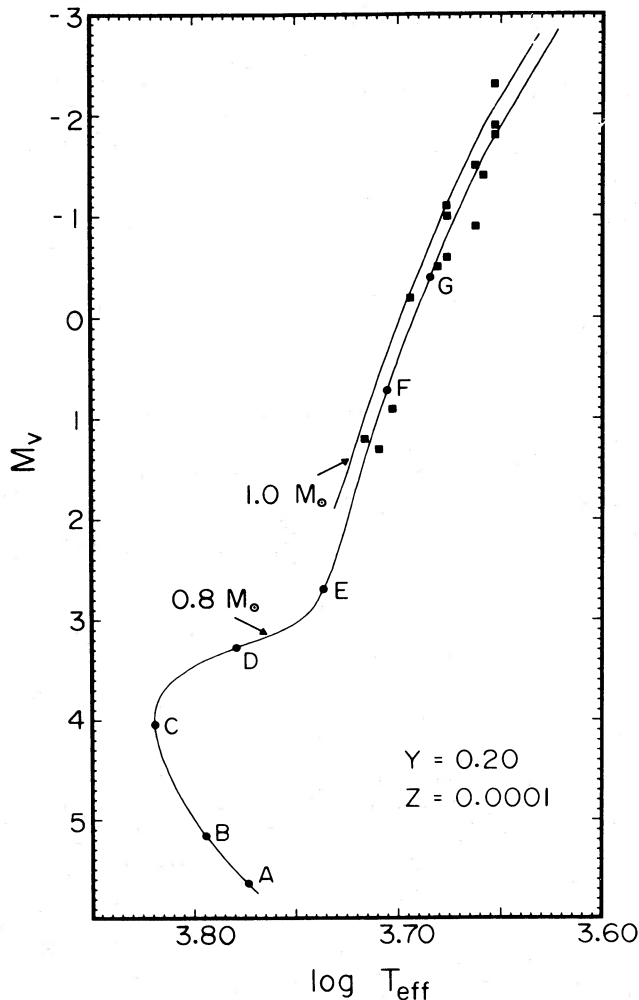


FIG. 7.—Evolutionary track for a $0.8 M_{\odot}$ star from the zero-age main sequence to the helium flash point, along with the red giant branch for a $1.0 M_{\odot}$ star. Filled circles indicate the locations of a number of models which are identified in Table 7, while filled squares give the positions of the observed Population II giants listed in Table 4.

TABLE 7
SELECTED MODELS ALONG $0.8 M_{\odot}$, $Y = 0.2$, $Z = 10^{-4}$
EVOLUTIONARY SEQUENCE

Model (1)	Age (2)	$\log L$ (3)	$\log T_{\text{eff}}$ (4)	$\log g$ (5)	$\log T_c$ (6)	$\log \rho_c$ (7)	M_{env} (8)	M_{sh} (9)
A	2.385	-0.319	3.7737	4.701	7.089	2.033	0.796	...
B	9.222	-0.136	3.7936	4.598	7.167	2.349	0.798	0.020
C	16.332	+0.300	3.8191	4.263	7.362	3.180	0.800	0.147
D	17.748	+0.626	3.7786	3.776	7.460	4.220	0.794	0.191
E	18.000	+0.873	3.7366	3.361	7.539	4.820	0.586	0.200
F	18.290	+1.700	3.7050	2.407	7.635	5.393	0.352	0.285
G	18.338	+2.215	3.6825	1.802	7.721	5.624	0.382	0.348

metal-deficient field giants considered in this investigation (recall our derivation of the atmospheric parameters for the program stars as described in § IVa).

For the purposes of the present discussion, we have selected a number of models—denoted by the letters A–G—which are indicated in Figure 7 at various points along the $0.8 M_{\odot}$ sequence. The basic properties of these models are listed in Table 7, where columns (1)–(7) give, in turn, the model identification, the age (in units of 10^9 yr), and the logarithms of the luminosity, the effective temperature, the surface gravity, the central temperature, and the central density. The last two columns give, respectively, the mass interior to the inner boundary of the convective envelope (M_{env}) and the mass interior to the point where the hydrogen abundance is one-half of its surface value (M_{sh} , which defines the center of the H-burning shell, when one exists). Throughout this discussion, masses and luminosities are given in solar units, while cgs units are adopted for all other quantities.

In Figure 8 we show how the mass-fraction abundances of ^1H and the CNO elements vary throughout the $0.8 M_{\odot}$ star at the various times in its evolutionary history represented by models A–E. Also indicated in this figure are the values of M_{env} and M_{sh} for each of the five models. Clearly, no changes in the surface CNO abundances are predicted to have occurred prior to model E (at the base of the RGB) since the convective envelope, which reaches inward to only $M_r = 0.586 M_{\odot}$ at that point, is still well above the central regions of the star that have undergone nuclear processing.

From an inspection of Figure 8, it is immediately apparent that a peak in the ^{13}C abundance is produced during the early main-sequence life of the star. This arises because of the (initially assumed) large overabundance of ^{12}C compared to ^{13}C , which more than compensates for the fact that, at all temperatures, the rate per nucleon of the $^{12}\text{C}(p, \gamma)^{13}\text{N}(\beta + \nu)^{13}\text{C}$ reaction is slower than that of the $^{13}\text{C}(p, \gamma)^{14}\text{N}$ reaction. As a result, the rate per gram of the former is greater than that of the latter over a substantial portion of the stellar interior, leading to the production of ^{13}C and the rise of the abundance of this isotope above its surface value. However, at greater depths where the temperatures are higher and interaction lifetimes are shorter, ^{13}C is rapidly destroyed by conversion to ^{14}N .

Consequently, the abundances of both carbon isotopes fall below their surface values to levels which are consistent with CN equilibrium. The data in Figure 8 show that, in the ^{13}C peak itself, the $^{12}\text{C}/^{13}\text{C}$ ratio reaches ~ 2.5 , and that when the CN equilibrium is attained interior to this peak, nearly all of the carbon has been converted to nitrogen.

When the star reaches the main-sequence turnoff, the bluest

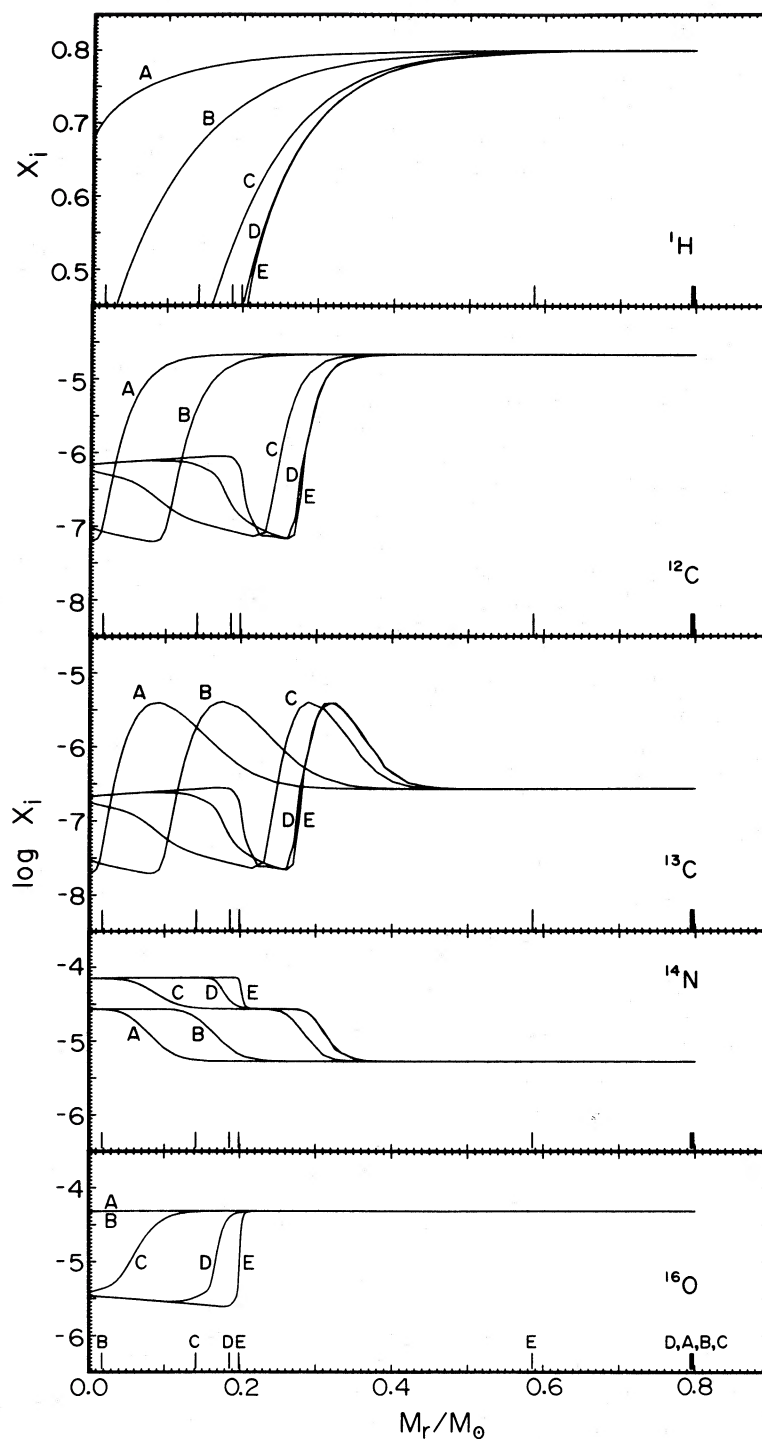


FIG. 8.—Interior abundance profiles of models A–E of the $0.8 M_{\odot}$ sequence. The lowermost panel associates with the models the vertical lines which have been plotted along the abscissa of each panel: those to the right of $M_r/M_{\odot} = 0.4$ indicate the location of the inner boundary of the convective envelope for various models, while those to the left indicate where the mass-fraction abundance of hydrogen has fallen to one-half of its surface value, X_1 . Only that part of the hydrogen profile above $0.5X_1$ has been plotted in the topmost panel.

point of the track, hydrogen in the core is exhausted. Thereafter, the star is supported by a hydrogen-burning shell which advances outward and steadily becomes thinner with time. A simultaneous expansion of the outer layers occurs which tends to narrow further the region where nucleosynthesis can proceed. As a result, the composition structure of the star above the H-burning shell no longer changes significantly (note the near coincidence of the abundance profiles of model D and E) until deep convective mixing can bring the material to the surface.

It is worth pointing out that while ON-cycling does not occur during the early evolution of a metal-poor $0.8 M_{\odot}$ star, equilibrium of the full CNO cycle is achieved in the late stages of core H-burning. By the time model C is reached, for instance, the oxygen abundance at the stellar center has fallen by an order of magnitude, giving rise to a double plateau in the ^{14}N abundance profile. The increased ^{14}N content leads, in turn, to higher abundances of the carbon isotopes in order to maintain consistency with CN equilibrium. Interestingly, the resultant ^{13}C abundance from full CNO-equilibrium cycling is nearly identical to the ^{13}C content initially assumed in the model.

According to standard stellar evolutionary theory, virtually all of the composition changes that are expected to occur as the result of convective dredge-up do so between models E and F. In Figure 9 we illustrate the CNO distributions of these two models, the former at the base of the RGB before any dredge-up has occurred, the latter at the point where the convective envelope has reached its maximum extent in terms of the amount of mass it encompasses. Looking at the left-hand panel of Figure 9 first, we see that the $^{12}\text{C}/^{13}\text{C}$ abundance ratio rises smoothly from ~ 3 in the region of CN equilibrium to the surface value of ~ 88 , which was assumed in the primordial mix. Since the inner boundary of the convective envelope never reaches deeper than $0.352 M_{\odot}$ (see the data for model F in Table 7), convection will never reach the ^{13}C peak which is located at $M_r = 0.32 M_{\odot}$. Consequently, one cannot expect a

significant lowering of the $^{12}\text{C}/^{13}\text{C}$ ratio as a result of the first dredge-up in this particular star. Indeed, as we see in the right-hand panel of Figure 9, the surface carbon isotope ratio is predicted to fall only to a value of 67.

Obviously, the location of the ^{13}C abundance peak will depend on the structure of the star on the main sequence. For example, one can expect that overall interior temperatures will tend to be hotter in a higher mass star, so that the ^{13}C peak will be displaced to a larger value of M_r/M_{\odot} . That this is borne out by the calculations is shown in Figure 10, which gives a plot of the composition profiles for 0.9 and $1.0 M_{\odot}$ stars having the same initial abundances and nearly the same evolutionary states (similar M_{sh} values) as model E of the $0.8 M_{\odot}$ sequence. What is particularly striking about this figure—taken together with the left-hand panel of Figure 9—is the tremendous sensitivity of the location of the ^{13}C abundance peak to the total stellar mass. In this particular example for masses of 0.8 , 0.9 , and $1.0 M_{\odot}$ respectively, the peak in the ^{13}C abundance profile is predicted to occur at $M_r = 0.32$, 0.38 , and $0.45 M_{\odot}$. Since, for a given metallicity, the depth of maximum penetration of the convective zone on the RGB is not a very sensitive function of the stellar mass (see Table 6), the $^{12}\text{C}/^{13}\text{C}$ ratio will necessarily be smaller in higher mass stars. For example, the convective envelope in a $1.0 M_{\odot}$ star will eventually extend down to $M_r = 0.365 M_{\odot}$, which is well below the ^{13}C abundance peak. In this case, the first dredge-up produces significant surface abundance changes, lowering the $^{12}\text{C}/^{13}\text{C}$ ratio from 88 to 29 and reducing the C/N ratio by a factor of ~ 1.5 . The predicted tendency toward lower $^{12}\text{C}/^{13}\text{C}$ ratios in stars of higher metallicity also is explained easily by the fact that convective envelopes will reach deeper into more metal-rich stars (see Table 6).

At first sight it would appear that the $^{12}\text{C}/^{13}\text{C}$ ratio has excellent potential for estimating the masses, and hence, the ages of stars evolving along the lower RGB. However, it is clear from the above discussion that any extra mixing (e.g., convective overshooting) would have some effect on the pre-

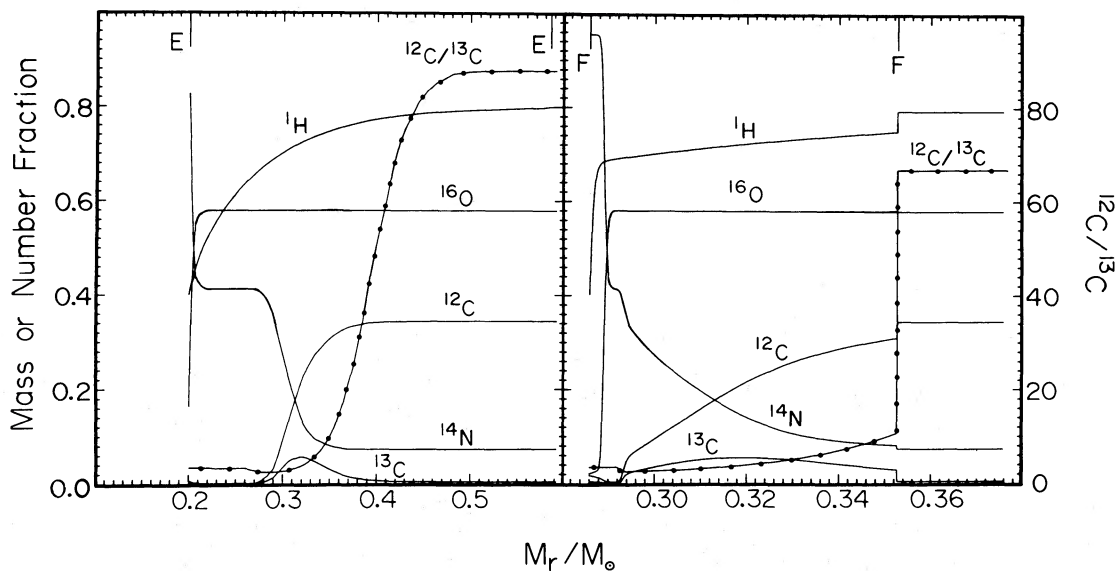


FIG. 9.—Distribution of the CNO elements between the center of the hydrogen-burning shell and the convective envelope of models E (left-hand panel) and F (right-hand panel). Right vertical scale gives the $^{12}\text{C}/^{13}\text{C}$ number abundance ratio, while that to the left gives the mass-fraction abundance of hydrogen or, in the case of ^{12}C , ^{13}C , ^{14}N , and ^{16}O , the number of each species as fractions of the total number of CNO nuclei. Vertical lines along the upper abscissa give the location of the inner boundary of the convective envelope (to the right) and the point where the hydrogen abundance has fallen to one-half of its surface value (to the left).

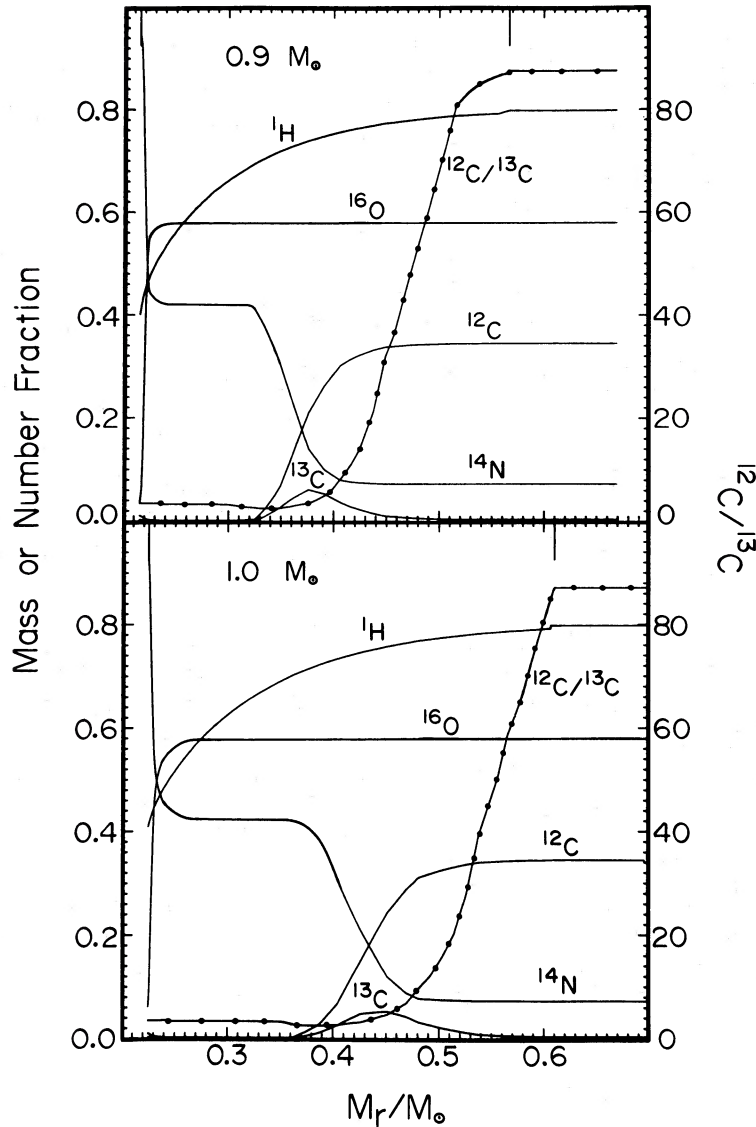


FIG. 10.—Similar to Fig. 9; in this case, the composition profiles are those of a $0.9 M_{\odot}$ star (top) and a $1.0 M_{\odot}$ star (bottom) at evolutionary phases which are similar to that of model E of the $0.8 M_{\odot}$ sequence.

dicted carbon isotope ratios of $0.8\text{--}0.9 M_{\odot}$ stars. To examine this possibility, numerical experiments were carried out on model F of the $0.8 M_{\odot}$ sequence, whereby arbitrary amounts of additional mixing on the surface abundances were determined. These show that overshooting by one pressure scale height, H_p , beyond the point of maximum penetration of the convective envelope, will alter the surface $^{12}\text{C}/^{13}\text{C}$ ratio by $\sim 20\%$ (i.e., it will drop from 67 to 53). Extra mixing by 2 or $3H_p$'s, for which there is no theoretical justification, will lower the surface carbon isotope ratio to values of 44 and 40, respectively. It therefore appears that the sensitivity of the predicted $^{12}\text{C}/^{13}\text{C}$ ratio to the stellar mass will not be destroyed by any reasonable amount of additional mixing. This point should be remembered if and when it becomes feasible to measure ^{13}C abundances of subgiants in populous star clusters where stellar masses and ages will be nearly identical.

With regard to our observations, the first dredge-up mixing phase may explain successfully the $[\text{C}/\text{Fe}]$ and $^{12}\text{C}/^{13}\text{C}$ values

only for the three least evolved stars of the present sample, which are the warmest and possess the lowest luminosities (HD 108317, HD 128279, and HD 175305). With the aid of the entries in Table 6 and with appropriate bolometric corrections (e.g., Bell and Gustafsson 1978) we have indicated in Figures 4 and 5 the approximate luminosity for completion of the first dredge-up in our stars ($M_v \approx +0.5$). (Actually, inspection of the computed evolutionary sequences shows that the inner boundary of the convective envelope changes only very slowly over ~ 0.6 mag on the RGB before reaching its maximum depth. In other words, the first dredge-up is already essentially complete by the time luminosities ~ 0.6 mag fainter than those listed in Table 6 are attained.) The three stars with lower luminosities than the indicated M_v boundary show reasonably good agreement with the prediction of little envelope processing. We note that, in addition to the relatively large carbon isotope ratios found in this study, these stars also were found by K82 to have fairly large amounts of carbon, and high C/N

ratios (see Fig. 6 and Table 4), consistent with the first dredge-up predictions of V86.

c) Speculation and Discussion

The presence of a large fraction of program giants with very low carbon isotope ratios argues for the need for more circulation of the envelopes of Population II red giants into a region where CN-cycle processing can take place. The arguments presented in the preceding section show that ordinary first dredge-up envelope abundance modifications cannot produce very low surface carbon isotope ratios observed in metal-poor giants. There exists only a very small mass region in the model interiors (see, for instance, Fig. 10) in which both $^{12}\text{C}/^{13}\text{C}$ ratios are very low and ^{12}C is still large. Since the fall of $^{12}\text{C}/^{13}\text{C}$ to its equilibrium value is followed quickly by the conversion of nearly all carbon to nitrogen, it is clear that the mixing of such material into the envelope will not lower the $^{12}\text{C}/^{13}\text{C}$ ratio sufficiently. In fact, it is for this very reason the $^{12}\text{C}/^{13}\text{C}$ ratios tend to asymptotically approach a value of ~ 28 at higher mass, independent of metal abundance.

Therefore, an additional mixing mechanism must be invoked to explain the abundance pattern in higher luminosity metal-poor giants, which exhibit very low $^{12}\text{C}/^{13}\text{C}$ values and (for some stars) greatly depleted overall carbon abundances. Sweigart and Mengel (1979) suggested that meridional circulation currents, driven by internal stellar rotation, could exist in low-mass giants. They demonstrated that a region of significantly depleted carbon, and low $^{12}\text{C}/^{13}\text{C}$, exists above the hydrogen burning shell of a red giant. An analogous diagram to their Figure 1 is given in Figure 11, which illustrates the distribution of the CNO elements in the vicinity of the H-burning shell for our $0.8 M_{\odot}$ model at approximately point G on the H-R diagram shown in Figure 7. At this evolutionary phase, the H-burning shell has already passed the composition discontinuity produced during the first dredge-up so that the gradient in the mean molecular weight, μ , which previously

existed above the shell (see the right-hand panel of Fig. 9), is now negligible in the region where CNO-cycling is occurring. Therefore, the μ barrier to slow circulation currents is no longer present. Note that, as suggested by Sweigart and Mengel, even a layer of depleted oxygen is predicted to exist above the H-burning shell in low mass metal-poor giants.

The approximate luminosities of onset of meridional circulation currents are given in the sixth column of Table 6 for a wide range in mass and metallicity. In general, these tend to be ~ 0.1 mag fainter than the predictions of Sweigart and Mengel. However, whereas our tabulation gives the luminosities where the top of the H-burning shell contacts the composition discontinuity, that by Sweigart and Mengel gives the values of $\log L$ when $M_{\text{sh}} = M_{\text{env}}(\text{max})$. Taking this into account essentially removes the discrepancy.

If circulation currents do operate in most metal-poor giants, then changes in the surface CNO abundances in addition to those induced in a star by the normal first dredge-up might be expected. Therefore, the meridional circulation onset luminosities of very anomalous CNO surface abundances. We define anomalous abundances here as $^{12}\text{C}/^{13}\text{C} < 28$ (Table 6), perhaps accompanied by low carbon abundances ($[\text{C}/\text{Fe}] < -0.5$), and small C/N ratios ($\log(\text{C}/\text{N}) < 0$). Evidently the predicted circulation onset magnitudes are fairly consistent with the observed appearance of $^{12}\text{C}/^{13}\text{C}$ anomalies (see Fig. 4, and note in Fig. 7 the location of model G relative to the observations). These magnitudes also are not very different from the giant-branch location where severe carbon depletions (see Fig. 5) and low C/N ratios appear. A cautionary note must be given here: a small group of metal-poor giants, without representation in our study, exhibit $\log(\text{C}/\text{N}) < 0$ at $+0.5 \geq M_v \geq 0.0$ (Fig. 5). However, most low C/N stars, including all of those in our sample, are brighter than $M_v \approx 0$.

Sweigart and Mengel (1979) did not make detailed calculations of the abundances of the CNO elements at the surfaces

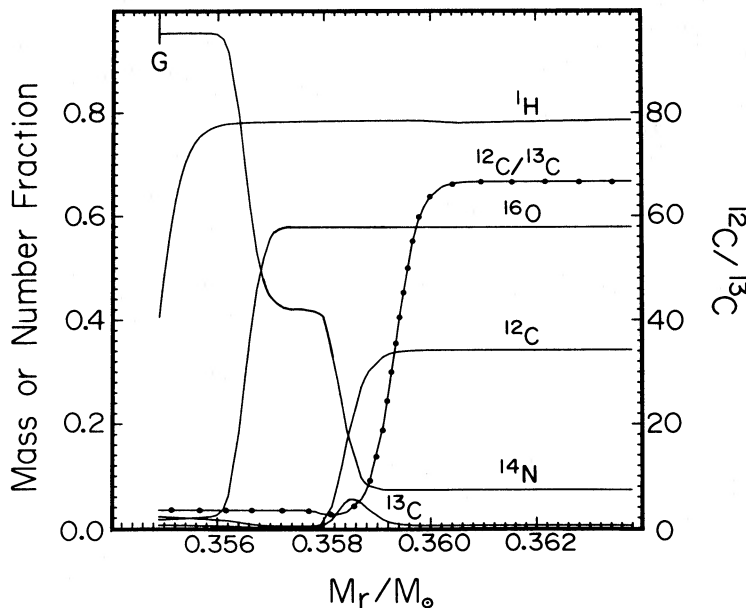


FIG. 11.—Similar to the Figs. 9 and 10; in this case, the composition profiles are those of the $0.8 M_{\odot}$ star considered in this study at a slightly more advanced phase of evolution than model G. Only the location of the center of the H-burning shell is indicated along the upper abscissa (by G). The inner boundary of the convective envelope of this model is located at $M_r \approx 0.385 M_{\odot}$.

of any of their model stars, and it is beyond our present capabilities to be able to do so here. However, we have performed a relatively simple calculation which seems to shed some light on the problem at hand. We have adopted the temperature, density, and abundance distributions of that particular $0.8 M_{\odot}$ model whose composition profiles are plotted in Figure 11, arbitrarily mixed the *entire* envelope above selected layers in the vicinity of the H-burning shell, and determined the amount of nucleosynthesis that would occur in the mixed region over a specified period of time. The region *below* the (arbitrarily enlarged) convective envelope was ignored, as was the energy liberated by the nuclear burning within the mixed region, so that the original temperature and density profiles as a function of M_r remained constant with time.

In Table 8 we give the results of this exercise for an assumed time step of 5×10^6 yr, which, at the location of model G in Figure 7 would be the time required for the star to evolve about 0.2 mag brighter. This seemed to be a reasonable choice, since the observations listed in Table 4 indicate that some stars can develop low $^{12}\text{C}/^{13}\text{C}$ ratios at luminosities which are very near to those where the onset of meridional circulation might be expected. The first and second columns list, respectively, the adopted inner boundaries of the mixed envelope structures and the temperatures at those values of M_r/M_{\odot} . The remaining four columns give the results of the nucleosynthesis calculation. Note that the factor by which ^{12}C is depleted is not, for many entries, identical to the increase in ^{14}N because of some redistribution of ^{12}C into ^{13}C . In addition, when most of the C has been converted to N, near equivalence of the absolute values of $[\text{C}/\text{Fe}]$ and $[\text{N}/\text{Fe}]$ should not be expected since the nitrogen content must level off at a value approaching $[\text{N}/\text{Fe}] = +0.7$, while the carbon abundance can continue to decline to very small values. The entries of this table demonstrate the possibilities of surface changes in the abundances. For example, if the mixed region were to extend down to $M_r = 0.3600 M_{\odot}$, which still is outside the region of significant CN cycling (see Fig. 11), then the amount of nucleosynthesis that would occur over a period of 5×10^6 yr would be negligible. On the other hand, if the entire envelope above $M_r = 0.3583 M_{\odot}$ (approximately the location of the ^{13}C abundance peak; again see Fig. 11) were to become mixed, then in 5×10^6 yr the surface $^{12}\text{C}/^{13}\text{C}$ would fall to a value of ~ 11 . Therefore the results of Table 8 give a very approximate estimate of the surface CNO abundances that would be produced by the continuous processing of a stellar envelope which accesses the nuclear burning regions in the interior.

Qualitatively, the results are in good accord with observational data. In fact, the observed abundance patterns of such stars as HD 88609, HD 115444, HD 122563, and HD 221170

(Table 4) bear a striking resemblance to the predicted $[\text{C}/\text{Fe}]$, $[\text{N}/\text{Fe}]$, $\log(\text{C}/\text{N})$, and $^{12}\text{C}/^{13}\text{C}$ ratios from our simplistic simulation. As mentioned previously, low values of the carbon isotope ratio are seen at the stellar surfaces for a wide variety of carbon depletions (and nitrogen enhancements). This is expected because the C/N ratio continues to fall toward the central regions of a model star while the $^{12}\text{C}/^{13}\text{C}$ ratio stays at the equilibrium value. The results contained in Table 8 suggests that deep mixing and processing will reduce the surface carbon isotope ratio to very low values (< 10) prior to severe reduction of C/N. The reason(s) for this mixing are not known yet, although ongoing circulation currents presently seem to be the most likely mechanisms.¹

While Sweigart and Mengel's (1979) general scheme to produce extra mixing appears sound, some modification in detail may be required. For instance, plots of the K82 values of C/N versus the stellar absolute magnitudes reveal no evidence of a continuing decline of C/N with luminosity above $M_b \approx -0.5$, which is approximately where the onset of circulation current mixing is predicted to commence (see Table 6). This suggests that the noncorrelation of $^{12}\text{C}/^{13}\text{C}$ with C/Fe or C/N may be due to variations in interior temperatures or in the efficiency of mixing of protons instead of variations in the length of time since circulation currents began, or the speeds of the currents.

Alternative scenarios for the explanations of varying amounts of CN cycling, such as mass loss and hydrogen shell instabilities (see Dearborn, Eggleton, and Schramm 1976; Harris and Lambert 1984) also should be kept in mind. In addition, as discussed by LK84, there may be the possibility of age and Z_{CNO} correlations with the degree of CN-cycle processing. We cannot add to their treatment on the age question, for a spread in Population II giant ages cannot be tested observationally. Their discussion of Z_{CNO} centered on possible correlations of the oxygen contents and the C/N ratios of Population II stars. They concluded simply that the oxygen data were too few to permit any meaningful analyses of this point. We have attempted a similar correlation between our $^{12}\text{C}/^{13}\text{C}$ ratios and the oxygen abundances given in some recent metal-poor star abundance papers (Leep and Wallerstein 1981; Gratton 1985). No trends are discernible for our five stars which have known oxygen abundances.

It is hoped that the present investigation will motivate further work to try to unravel the puzzling abundance data for giants of all metallicities that are being reported in this and similar studies. A very useful next step on the theoretical side would be to follow the evolution of red giants were deep mixing is artificially induced to see if it is possible (and what is required) to reproduce the wide variety of observed surface abundances. Such modeling could allow us to assess the sensitivity of the predicted abundance patterns to the particular

TABLE 8

PREDICTED ABUNDANCES FROM CN PROCESSING OF THE ENVELOPE OF A $0.8 M_{\odot}$ RED GIANT

M_r	$\log T$	$[\text{C}/\text{Fe}]$	$[\text{N}/\text{Fe}]$	$\log(\text{C}/\text{N})$	$^{12}\text{C}/^{13}\text{C}$
0.3600.....	7.157	0.00	0.00	+0.67	67.
0.3594.....	7.217	+0.00	0.00	+0.67	64.
0.3590.....	7.255	+0.00	0.00	+0.67	51.
0.3586.....	7.295	-0.02	0.01	+0.65	24.
0.3583.....	7.322	-0.04	0.04	+0.60	11.
0.3580.....	7.353	-0.16	0.23	+0.29	4.2
0.3578.....	7.374	-0.37	0.48	-0.18	2.8
0.3577.....	7.385	-0.58	0.61	-0.52	2.6
0.3576.....	7.397	-0.96	0.70	-1.00	2.5

¹ Unfortunately, the stellar rotations proposed by Sweigart and Mengel to drive the meridional circulation current probably are unobservable in Population II giants. Theoretically, the assumption of envelope constant specific angular momentum in a model giant was considered by Swigart and Mengel to be more realistic than the assumption of envelope solid-body rotation, but it led to very small ($\leq 0.1 \text{ km s}^{-1}$) surface rotational velocities. The larger velocities are expected to be seen only after substantial envelope mass loss, when a Population II giant is on the horizontal branch, and recent rotational studies have concentrated on those stars (Peterson, Tarbell, and Carney 1983). Finally, most observational efforts on red giant rotation among Population I stars have found undetectably small values for the surface velocities (e.g., see Smith and Dominy 1979).

level in the H-burning shell that is accessed, to the total stellar mass, to the initial helium content, and to the initial CNO abundances. That exercise might allow some constraints to be placed on the viability of the meridional circulation mechanism and/or on the properties of real stars. Observationally, some further determinations of $^{12}\text{C}/^{13}\text{C}$ ratios in Population II giants with extreme locations in the C/N versus M_v plane (as determined by K82) would help further define the location of onset and efficiency of the extra mixing demanded by our results and those of K82. Finally, we note again the paucity of oxygen abundance determinations in these stars, and the possibility that internal evolutions of metal-poor giants may act to deplete the surface abundances of this element.

VI. CONCLUSIONS

We have derived carbon isotope ratios or lower limits to those ratios for 15 very metal-poor giants. We have shown that the isotope ratios in these stars often are very low, and tend to

decrease with increasing luminosities of the giants. The existence of very low values of $^{12}\text{C}/^{13}\text{C}$ is shown to be inconsistent with detailed abundance predictions for the first dredge-up in low-metallicity stellar models. Some additional mixing between the envelopes and the CN-cycled interior layers must be postulated to produce the low carbon isotope ratios and the low C/N values of Population II giants determined in other studies. Order-of-magnitude calculations have been carried out to demonstrate that such extra mixing may be accomplished, although the precise mechanism for inducing the mixing remains uncertain at the present time.

We thank Robert Kraft, Beatrice Barbuy, Robert Rood, David Lambert, and Verne Smith for helpful discussions, and are grateful to Robert Rood for communicating some of his results to us in advance of publication. This work has been supported by National Science Foundation grants AST-8100241 and AST-8507934 to C. S.

REFERENCES

- Arnett, W. D. 1978, *Ap. J.*, **219**, 1008.
 Barbuy, B. 1981, *Astr. Ap.*, **101**, 365.
 ———. 1983, *Astr. Ap.*, **123**, 1.
 Bell, R. A., Eriksson, K., Gustafsson, B., and Nordlund, A. 1976, *Astr. Ap. Suppl.*, **23**, 37.
 Bell, R. A., and Gustafsson, B. 1978, *Astr. Ap. Suppl.*, **34**, 229.
 Bond, H. E. 1980, *Ap. J. Suppl.*, **44**, 517.
 Carbon, D. F., Barbuy, B., Kraft, R. P., Friel, E., and Suntzeff, N. 1986, *Pub. A.S.P.*, in preparation.
 Carbon, D. F., Langer, G. E., Butler, D., Kraft, R. P., Trefzger, C. F., Suntzeff, N., Kemper, E., and Romanishin, W. 1982, *Ap. J. Suppl.*, **49**, 207.
 Carney, B. W. 1979a, *Ap. J.*, **233**, 211.
 ———. 1979b, *Ap. J.*, **233**, 877.
 Chmielewski, Y. 1984, *Astr. Ap.*, **133**, 83.
 Cohen, J. G. 1979, *Ap. J.*, **231**, 751.
 Cohen, J. G., and Grasdalen, G. L. 1968, *Ap. J. (Letters)*, **151**, L41.
 Cottrell, P. S., and Sneden, C. 1986, *Astr. Ap.*, in press.
 Day, R. W., Lambert, D. L., and Sneden, C. 1973, *Ap. J.*, **185**, 213.
 Dearborn, D. S. P., Eggleton, P. P., and Schramm, D. N. 1976, *Ap. J.*, **203**, 455.
 Delbouille, L., Neven, L., and Roland, G. 1973, *Photometric Atlas of the Solar Spectrum from 3800 to 10 000 Å* (Liège: Université de Liège).
 Gratton, R. G. 1985, preprint.
 Griffin, R., Griffin, R., Gustafsson, B., and Vieira, T. 1982, *M.N.R.A.S.*, **198**, 637.
 Gustafsson, B., Kjergaard, P., and Andersen, S. 1974, *Astr. Ap.*, **34**, 99.
 Harris, M. J., and Lambert, D. L. 1984, *Ap. J.*, **285**, 674.
 Holweger, H., and Müller, E. A. 1974, *Solar Phys.*, **39**, 19.
 Iben, I., Jr., and Renzini, A. 1984, *Phys. Letters*, **105**, 329.
 Kjergaard, P., Gustafsson, B., Walker, G. A. H., and Hultqvist, L. 1982, *Astr. Ap.*, **115**, 145.
 Kraft, R. P. 1985, in *Production and Distribution of CNO Elements in the Galaxy*, ed. I. J. Danziger, F. Matteucci, and K. Kjær (Garching bei München: ESO), p. 21.
 Kraft, R. P., Suntzeff, N. B., Langer, G. E., Carbon, D. F., Trefzger, C. F., Friel, E., and Stone, R. P. S. 1982, *Pub. A.S.P.*, **94**, 55.
 Krupp, B. M. 1974, *Ap. J.*, **189**, 389.
 Kurucz, R. L., and Peytremann, E. 1975, *SAO Spec. Rept.*, No. 362.
 Laird, J. B. 1985, *Ap. J.*, **289**, 556.
 Lambert, D. L. 1978, *M.N.R.A.S.*, **182**, 249.
 Lambert, D. L., and Dearborn, D. S. 1972, *Mem. Soc. Sci. Roy. Liège*, 6^e Ser. **3**, 147.
 Lambert, D. L., and Mallia, E. A. 1968, *Ap. Letters*, **1**, 85.
 Lambert, D. L., and Ries, L. M. 1981, *Ap. J.*, **248**, 228.
 Lambert, D. L., and Sneden, C. 1977, *Ap. J.*, **215**, 597.
 Lambert, D. L., Sneden, C., and Ries, L. M. 1974, *Ap. J.*, **188**, 97.
 Langer, G. E. 1985, *Pub. A.S.P.*, **97**, 373.
 Langer, G. E., and Kraft, R. P. 1984, *Pub. A.S.P.*, **96**, 339.
 Langer, G. E., Kraft, R. P., and Friel, E. D. 1985, *Pub. A.S.P.*, **97**, 382.
 Leep, E. M., and Wallerstein, G. 1981, *M.N.R.A.S.*, **196**, 543.
 Luck, R. E., and Bond, H. E. 1981, *Ap. J.*, **244**, 919.
 Meggers, W. F., Corliss, C. H., and Scribner, B. F. 1975, *NBS Monog.*, No. 145.
 Moore, C. E., Minnaert, M. G. J., and Houtgast, J. 1966, *NBS Monog.*, No. 61.
 Norris, J., and Pilachowski, C. A. 1985, *Ap. J.*, **299**, 295.
 Pagel, B. E. J. 1964, *Roy. Obs. Bull.*, No. 87.
 Peterson, R. C., Tarbell, T. D., and Carney, B. W. 1983, *Ap. J.*, **265**, 972.
 Smith, M. A., and Dominy, J. F. 1979, *Ap. J.*, **231**, 477.
 Sneden, C. 1973, *Ap. J.*, **184**, 839.
 ———. 1974, *Ap. J.*, **189**, 493.
 ———. 1983, *Pub. A.S.P.*, **97**, 747.
 ———. 1985, in *Production and Distribution of CNO Elements in the Galaxy*, ed. I. J. Danziger, F. Matteucci, and K. Kjær (Garching bei München: ESO), p. 1.
 Sneden, C., and Parthasarathy, M. 1983, *Ap. J.*, **267**, 757.
 Sneden, C., and Pilachowski, C. A. 1985, *Ap. J. (Letters)*, **288**, L55.
 Sweigart, A. V., and Mengel, J. G. 1979, *Ap. J.*, **229**, 624.
 Tomkin, J., and Lambert, D. L. 1984, *Ap. J.*, **279**, 220.
 Tomkin, J., Sneden, C., and Lambert, D. L. 1986, *Ap. J.*, **302**, 415.
 Tull, R. G., Choisser, J. P., and Snow, E. H. 1975, *Appl. Optics*, **14**, 1182.
 Uomoto, A. K. 1981, Ph.D. thesis, University of Texas at Austin.
 VandenBerg, D. A. 1984, in *IAU Symposium 105, Observation Tests of the Stellar Evolution Theory*, ed. A. Maeder and A. Renzini (Dordrecht: Reidel), p. 143.
 ———. 1986, in preparation.
 VandenBerg, D. A., and Bell, R. A. 1985, *Ap. J. Suppl.*, **58**, 561.
 Vogt, S. S., Tull, R. G., and Kelton, P. 1978, *Appl. Optics*, **17**, 574.
 Wagoner, R. B., Fowler, W. A., and Hoyle, F. 1967, *Ap. J.*, **148**, 3.
 Wilson, O. C. 1976, *Ap. J.*, **205**, 823.

CATHERINE A. PILACHOWSKI: Kitt Peak National Observatory, National Optical Astronomy Observatories, Box 26732, Tucson, AZ 85726-6732

CHRISTOPHER SNEDEN: Department of Astronomy and McDonald Observatory, University of Texas, Austin, TX 78712

DON A. VANDENBERG: Physics Department, University of Victoria, Box 1700, Victoria, B.C. V8W 2Y2, Canada